CHAPTER FOUR

WIDEBAND MIMO MEASUREMENT SYSTEM

4.1 INTRODUCTION

For many realistic environments and systems, limited multipath or compact arrays lead to channels with non-Rayleigh iid statistics. Research in MIMO channel characterization and modelling [90, 91] indicates that MIMO channels have very complicated behavior that is only captured by direct measurement (see [19] and references therein). Although theoretical channel capacity may be insensitive to the exact structure of the channel, realistic system design may depend heavily on this structure. For example, double-directional clustering observed in measured channels suggests the advantage of directional elements [47]. Space-time codes designed with an understanding of the channel structure can outperform codes designed with the iid assumption [7]. Furthermore, performance in realistic scenarios with multiple users may depend more heavily on channel structure than the single-user channel [92]. Since a detailed understanding of the channel behavior is required for optimal system design and accurate performance assessment, direct measurement of MIMO channels continues to be important. To partially fill the gap between the high cost of commercial channel sounders and the long time associated with in-house development, a new low-cost wideband MIMO channel sounder has been developed. It is operationally similar to commercial sounders [93], and can be constructed at moderate cost by leveraging conventional off-the-shelf components (COTS), instruments and modules. The purpose of developing this low-cost channel sounder was to obtain indoor channel data for modelling research presented in this thesis. The objective of this chapter is to give the reader an overview of the developed and deployed system. The reader can refer to other sources

such as [88, 94, 95] for more detail should anyone wish to develop such a system.

4.2 SYSTEM OVERVIEW

The design goals that were envisioned with the channel sounder at the University of Pretoria are:

- *Rapid Development*

The idea was that measurement equipment, instruments and mainly off-the-shelf components should be used so that the system development time and risk are reduced. With the experience and expertise available such a system can be deployed within six to eight months.

- *Affordability*

Considering the financial constraints, the implemented system should be affordable to build and integrate.

- *Antenna Arrays*

The system should be capable of supporting up to a maximum of eight transmitters and receivers and the system should be flexible so that one could change the orientation of the antennas without much difficulty.

- *System Flexibility*

The components in the system should be flexible and modular, allowing easy reconfiguration for different measurement scenarios. It should be easily modified to accommodate outdoors and mobile measurement scenarios.

- *Frequency Range*

It was envisaged that one should be able to undertake measurements in the 2-8 GHz band as this seemed to be a band with greater focus of attention and relevance. However, measurements were taken at 2.4 GHz and 5.2 GHz carrier frequencies since these were in the ISM band and did not require any permission from the regulator to use them in South Africa. These two frequencies also provided a reasonable separation to base any of the frequency scaling issues discussed.

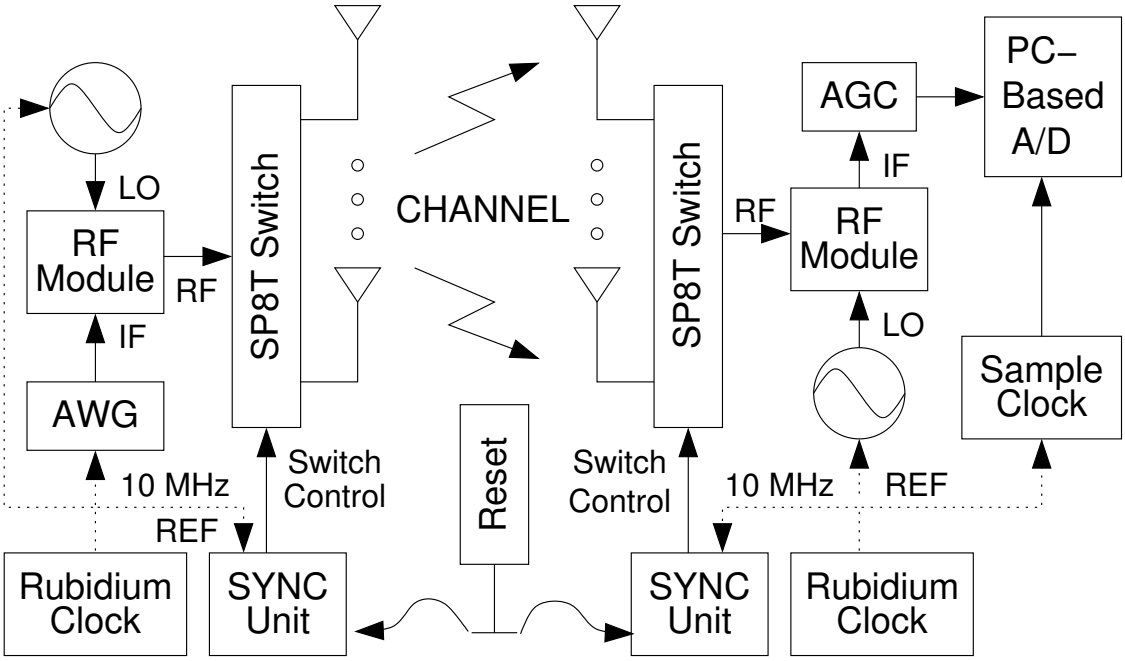

FIGURE 4.1: High level diagram of the wideband MIMO channel sounder

- *Bandwidth*

The intention was to be probing bandwidths in excess of 120 MHz but the instrumentation allowed only 80 MHz of instantaneous bandwidth. However this was considered sufficient in this study of current realistic wideband MIMO system communication signalling.

The system implemented is shown in Figure 4.1 with the popular ”switched array” architecture being employed where various antenna elements are connected to the TX and RX via high speed absorptive microwave switches. ”True array” techniques that measure multiple TX/RX channels simultaneously can also be employed but these tend to be expensive, they require longer development time and can complicate maintenance. With the availability of high speed absorptive microwave switches with switching times in the order of 25 ns, as well as having an off-time to take care of transients, the non-ideal response induced by the ”switched array” is negligible.

At the TX in the system shown in Figure 4.1, a radio frequency (RF) module mixes the wideband signal from the arbitrary generator (AWG) with the local oscillator (LO) to up-convert to the desired microwave carrier. This signal is fed into an RF power amplifier and then into a single pole eight-throw (SP8T) microwave switch to one of the eight TX antennas. At the

RX, the signals on the antennas are routed via another SP8T switch to an RF block, consisting of a low noise amplifier (LNA), a single stage down-conversion to an intermediate frequency (IF) and then through a low-pass filter (LPF). This IF signal is amplified by an automatic gain control (AGC) circuit and stored onto a computer hard disk drive using a high-speed PC-based A/D card (example GaGe). The accurate co-ordination of the switching of TX and RX arrays is accomplished by a custom-designed synchronization (SYNC) unit [94]. Timing in the system is referenced by highly stable 10MHz rubidium time/frequency oscillators, ensuring proper timing and phase coherence throughout the system.

4.3 SYSTEM COMPONENTS

This section outlines the respective hardware components used in the wideband MIMO channel sounder.

4.3.1 Transmitter Subsystem

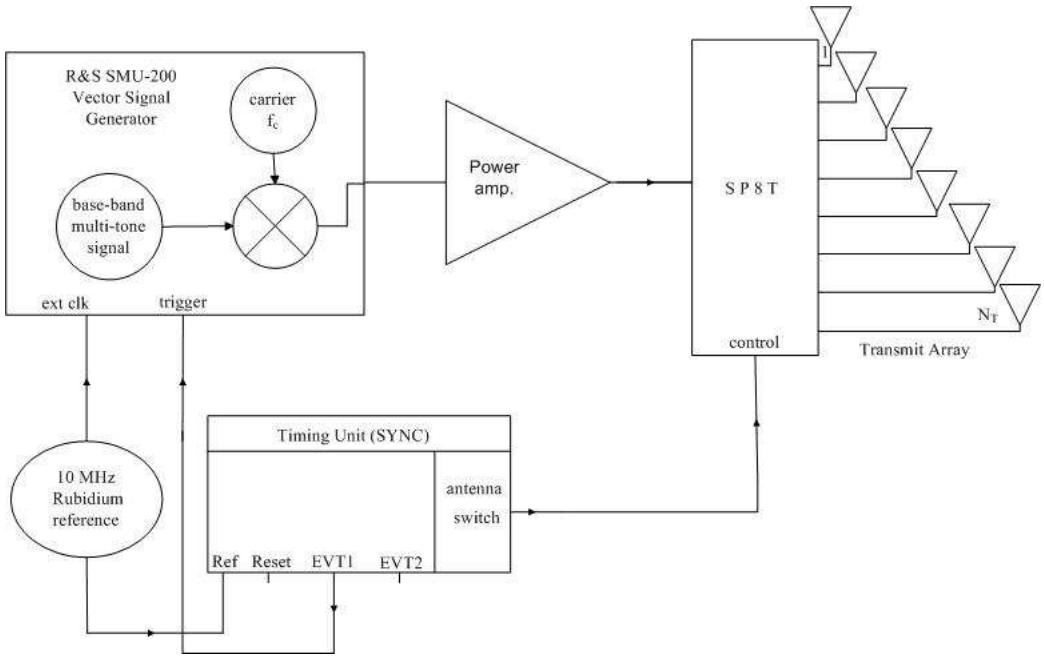

FIGURE 4.2: High level block diagram of the TX subsystem

The TX subsystem implemented at the University of Pretoria (UP) is shown in Figure. 4.2. This system is essentially used to sequentially excite the wireless channel across an instantaneous bandwidth of 80MHz for each of the N_T antennas. After generating a baseband

probing signal on the AWG, an RF module mixes this signal to the LO to up-convert to the microwave switch to one of eight outputs. In this implementation the Rohde & Schwarz SMU200 vector signal generator is used to generate the base-band signal and up-converts it to the desired microwave center frequency. This signal is then amplified by a high power RF amplifier and then fed into the SP8T microwave switch. Each of the eight antennas are connected to the SP8T. The SYNC unit supplies transistor-transistor-logic (TTL) enabled lines to the microwave switch and an event trigger releases timing bursts to the AWG located in the SMU200 unit.

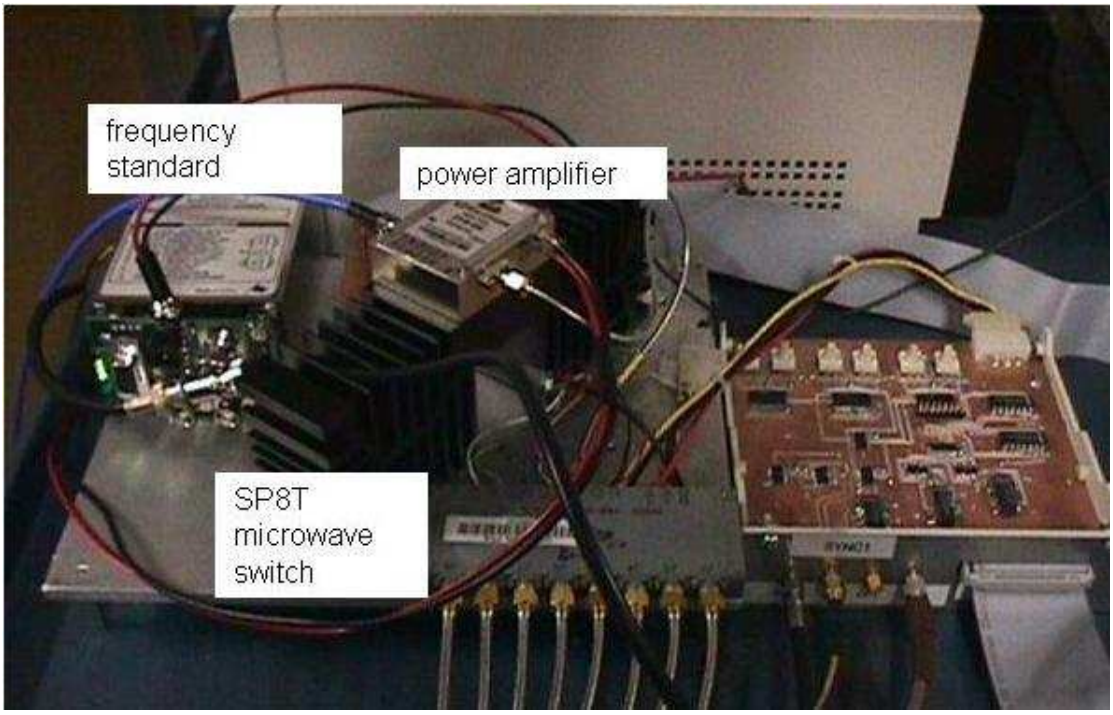

FIGURE 4.3: Transmit RF module

The RF module as shown in Figure 4.3 houses primarily the microwave components required for the up-conversion of the base-band probing signal to the microwave carrier and routing of the signal to the proper output antenna via the SP8T microwave switch.

4.3.2 Receiver Subsystem

Figures 4.4 and 4.5 show a block diagram of the RX subsystem, whose purpose is to sample the received wideband signal for $N_T \times N_R$ antenna combinations. For each combination, the RX-RF module routes the signal from one of the N_R RX antennas to a broadband 40 dB gain

LNA, followed by a mixer for a single-stage down conversion to an intermediate

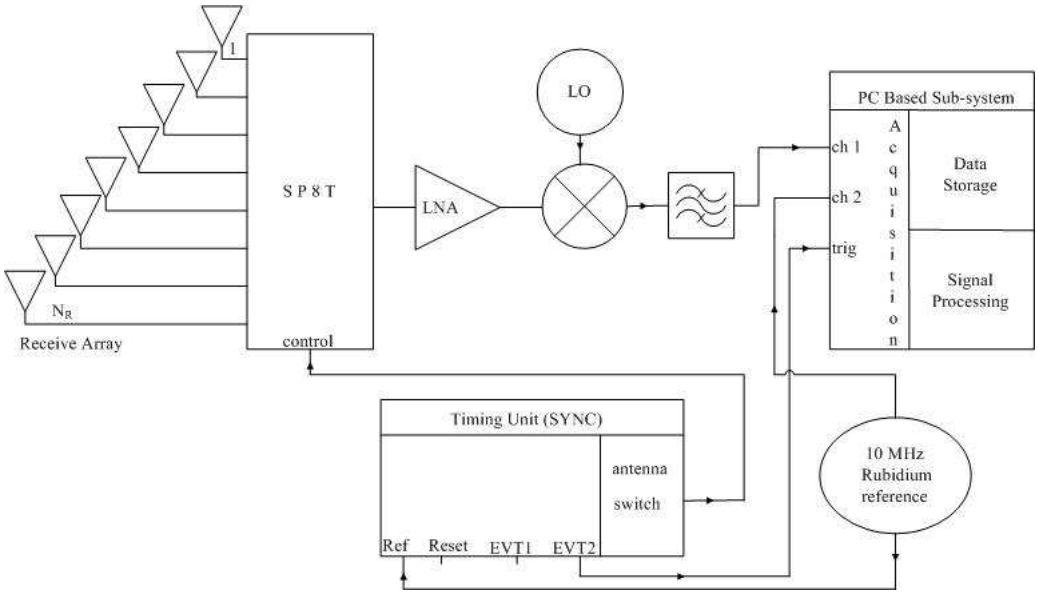

FIGURE 4.4: High level block diagram of the RX subsystem

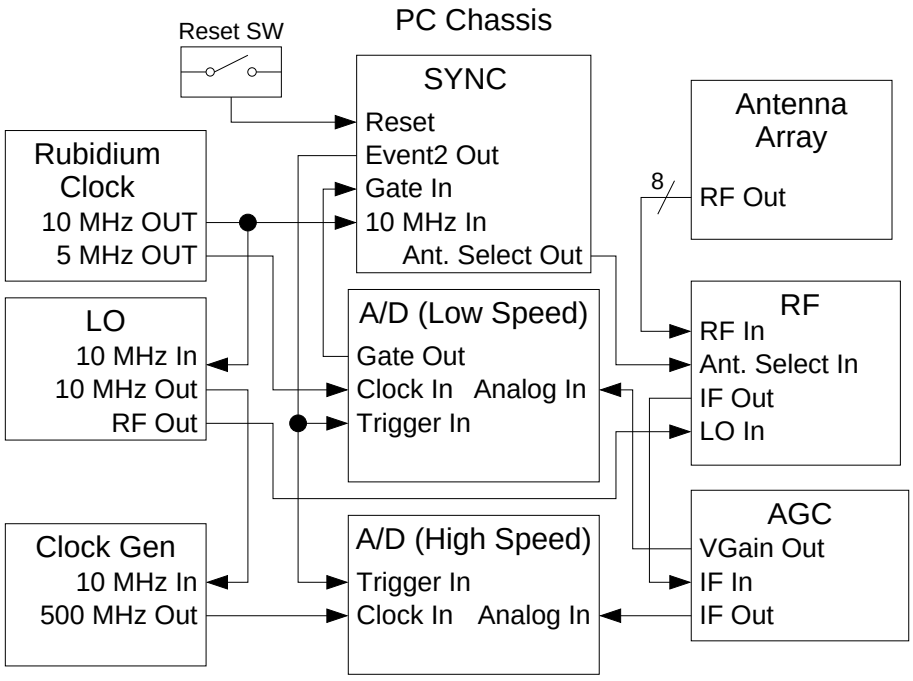

FIGURE 4.5: Block Diagram of the RX subsystem connections

frequency (IF) of 100 MHz. The IF signal is low-passed filtered, fed to the AGC module with 0-40 dB of IF gain, and sampled on a high speed 500 MSa/s analog-to-digital (A/D) card. The voltage gain signal of the AGC is a power detector output whose voltage is proportional to the signal in dB, and this signal is sampled by an inexpensive low-speed multifunction

input-output (I/O) (MIO) board.

The rate of switching on the SYNC unit is $1/N_T$ relative to the TX subsystem so as to allow the channel from all N_T transmitters to be measured for each of the N_R receivers. The high- and low- speed A/D boards (for measuring the wideband IF waveform and gain level respectively) are triggered simultaneously by the EVT1 (event1) signal, which is asserted for each complete scan of the N_R antennas.

The use of two A/D boards can create potential problems for triggering, since the software must sequentially arm the two boards, thus creating a critical section where one board can trigger while the other is not ready. To avoid this potential hazard, the SYNC unit has an additional Gate input, which, when negated, inhibits event outputs. Thus, Gate is first negated (using a digital output of the MIO board), the two cards are sequentially armed, and finally Gate is asserted. Subsequent event signals then trigger both boards simultaneously.

Although most instruments use the 10 MHz rubidium clock directly, the A/D boards require direct input of an external sample clock. A function (or clock) generator provides a 500 MHz sine wave signal to the high-speed A/D board, and an auxiliary 5 MHz square wave output on the rubidium oscillator drives the low-speed A/D board clock. A large change in the RX power level with movement or time is possible due to multipath fading and shadowing in a communications environment. In order to capture this, measurement sensitivity using an AGC circuit was implemented using a simple AD8367 based circuit that provides 0-40 dB of IF gain. The time constant of the AGC loop is approximately 5 μs, so that the gain can adapt for each new TX/RX pair. A fairly low-speed (1MS/s) A/D board samples the output voltage of the AGC loop, from which the gain can be computed and the true waveform recovered.

4.3.3 Synchronization Module

The key to the operation of the switched array technique in MIMO wideband channel sounding is the synchronization. There needs to be co-ordinated switching as at the TX the signal bursts and at the RX data acquisition needs to take place within a set time window. These tasks are accomplished by a synchronization unit (SYNC) as shown in Figure 4.7. This SYNC

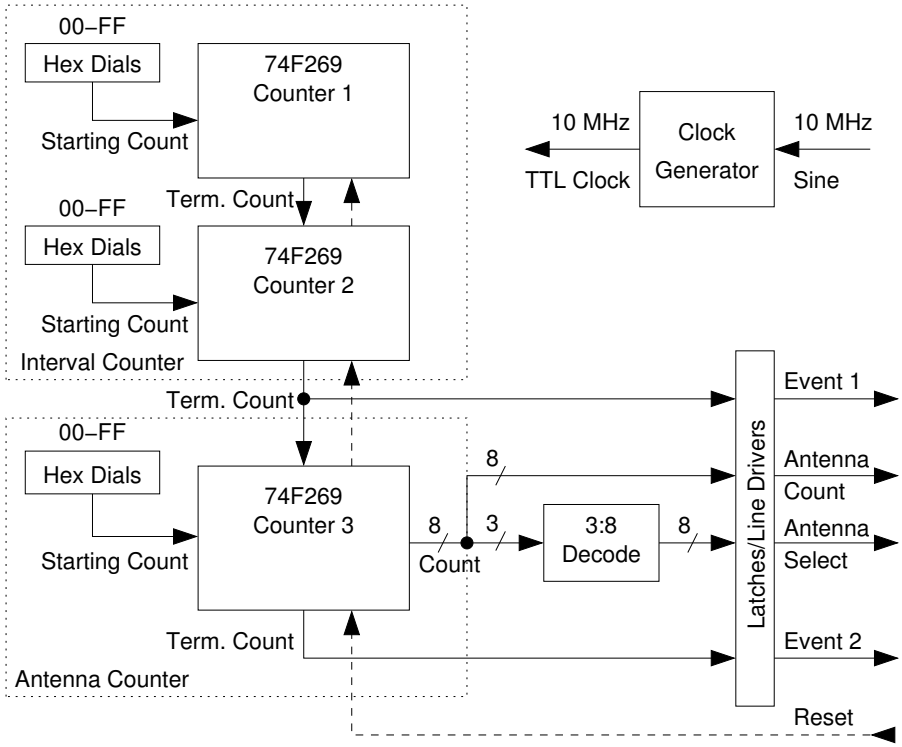

FIGURE 4.6: Simplified schematic of the SYNC unit

unit which was custom designed by Wallace [94] as no affordable COTS solution was then available, consists of counters operating at a rate of 10 MHz.

The unit provides antenna selection signals and event outputs required for antenna switching, namely the AWG and A/D triggering. Figure 4.6 shows a simplified schematic diagram of the synchronization module, which is driven by a single stable, high quality 10 MHz input derived from a Rubidium source as shown in Figure 4.10. The board assumes that the input signal is a 10 MHz sine wave, and the ”clock source” circuit converts this input to a 5 V TTL signal with a comparator. The inputs of the comparator are set to a quiescent level of 2.5 V with resistive voltage dividers. The positive comparator input is then capacitively coupled to the 10 MHz reference. Thus, positive and negative input levels correspond to 5 V and 0 V TTL outputs respectively. Note that the 10MHz input is left unterminated, thus presenting a high impedance and allowing another reference input to be connected in tandem.

As depicted, the SYNC board consists of three 8-bit counters (74F269) operating at 10 MHz. The three counters are arranged into a 16-bit “interval counter” that controls the dwell time on each antenna and an 8-bit “antenna counter” that cycles through the antennas. Thus,

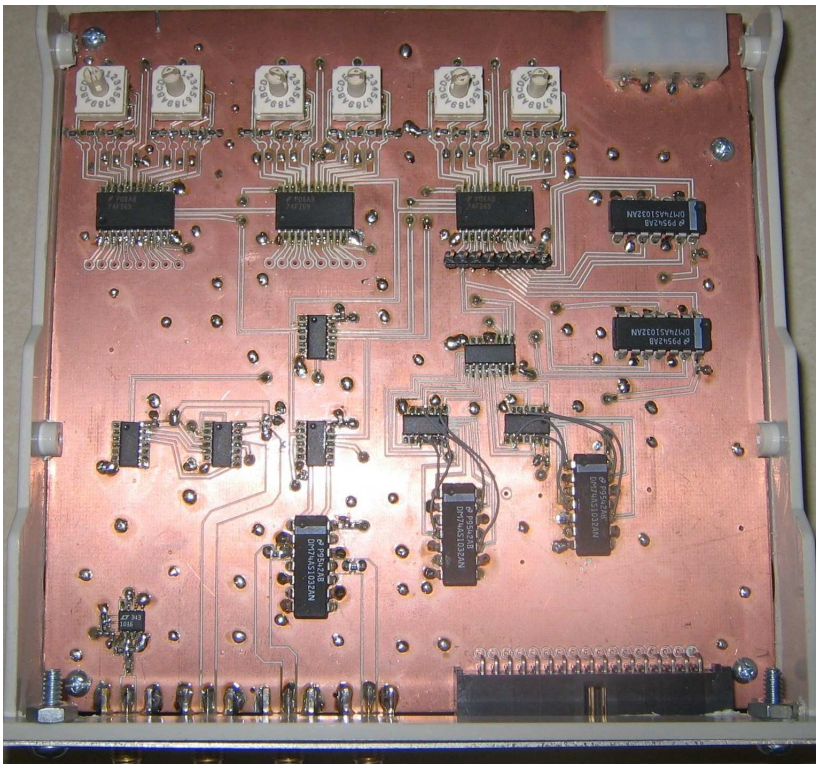

FIGURE 4.7: Top view of SYNC Unit

dwell times from 100 ns to 6.5 ms and antenna counts from 1 to 256 can be accommodated. The interval counter decrements on each clock cycle, and upon reaching the terminal count of zero, performs a parallel reload of its starting value, enables the antenna counter to decrement and asserts the terminal count (∼TC2) signal of counter 1. When both the interval and antenna counters simultaneously reach their terminal count, the antenna counter is also reloaded and the terminal count (∼TC3) signal from counter 2 is asserted. The initial values of both counters are currently set by hexadecimal dials, which should be set to the desired interval *minus one*. The dials are single-throw switches, and the outputs must be pulled down with 1 kΩ resistors on the board.

The 8-bit antenna counter value is fed via high-speed line drivers with a 100 Ω source termination to a ribbon cable connector. Since many commercial packaged PIN-diode switches have separate negative-logic enabled lines for each port, a 74F138 device decodes the three least-significant bits and provides the negative-logic strobe signals for the switches via line drivers to the ribbon cable interface. In this circuit, faster logic families, such as 74F and 74AS have been used to minimize propagation time and ensure smooth operation at 10 MHz. In order

to simplify triggering of AWG bursts and A/D conversion, event signals are also provided. The EVT1 signal is a synchronous and inverted version of the ∼TC2, thus asserting a pulse each time the interval counter resets. Likewise, the EVT2 signal, which is also shown in Figure 4.9, is derived from the ∼TC3 signal, providing a pulse when the antenna counter resets. The event signals are delivered by 50 Ω source-terminated line drivers fed to SMA type connectors.

Because the antenna counter counts in reverse order, the antenna outputs will be excited in descending order (for example for a 4-antenna measurement, the port excitation order is J4, J3, J2, J1). The reverse order must be accounted for either by reversing the order of connection to the array or by reversing the rows and columns of measured channel matrices during data processing.

The SYNC board is initially reset by an external reset switch connected to the reset (RST_SW) input. A temporary low signal on the RST_SW input creates a single reset pulse that causes the two counters to be loaded with their initial values. Figure 4.8 depicts a reset switch used to trigger two SYNC boards simultaneously. This very simple unit consists of a momentary switch that simultaneously shorts the two SMA cables to ground when the button is pressed. When the two cables are connected to two SYNC boards, this action causes the boards to begin counting at the same time.

Figures 4.7 and 4.9 show the top and front views of the completed SYNC module respectively. Here, the board has been mounted inside a 3.5” to 5.25” drive converter, which also gives one the option to conveniently integrate the unit into a computer chassis. One notices that the 10 MHz reference signal will be input and at the TX one will use EVT1 output for triggering, while at the RX one would use the EVT2 output for triggering while the microwave switches will be controlled by the outputs from ANTENNA SW so that respective switching configuration from TX-to-RX is active.

4.3.4 Monopole Antennas

The simple monopole antenna shown in Figure 4.11 and Figure 4.14 was used in the measurement system. It was mounted onto the grid plate shown in Figure 4.13 so as to produce reconfigurable antenna arrays.

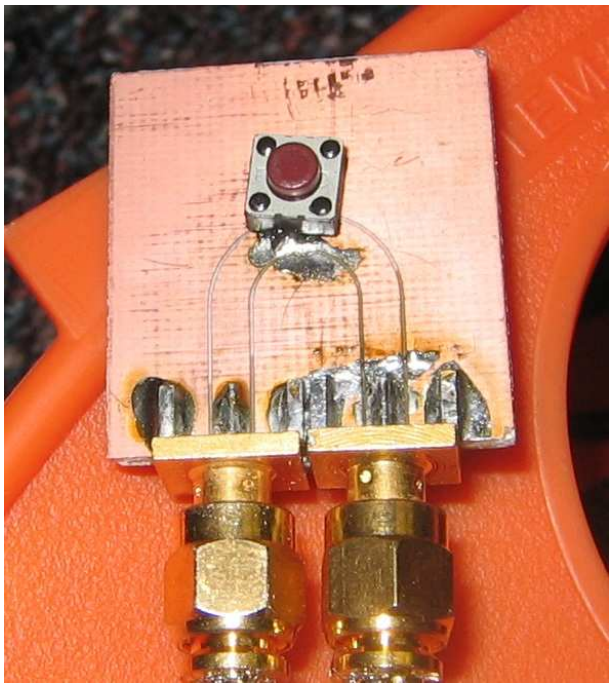

FIGURE 4.8: Reset/Trigger switch allowing simultaneous reset of two SYNC units

The design, layout and analysis of the single monopole antenna used in this system implementation is given in [96]. It was manufactured as shown in Figure 4.11, by soldering a copper whip to the center of a standard SMA bulkhead connector (Johnson part number 142-0901-401). A good 50Ω match was provisioned by providing an adequate length of the coaxial feed above the ground plane. The antennas were constructed for 2.4 GHz and 5.2 GHz center frequencies and the plots in [96] demonstrate that the antennas characteristics were adequate for implementation in this system.

The antennas were mounted on the grid plate shown in Figure 4.17, which also provided a very good ground plane. This novel method of implementation allowed for the flexibility in varying the element spacing as well as antenna array configuration for up to at least eight antenna elements as shown in example Figure 4.16. The spacing for the eight element circular array is $\lambda/2$ for both the 2.4 GHz and 5.2 GHz measurement campaign as shown in Figures 4.13 and 4.16 respectively. The linear array configuration shown in Figures 4.12 and 4.15 are for the implementation of the 2.4 GHz and 5.2 GHz respectively. Since the grid array was limited in physical size, an inter-element spacing of $\lambda/3$ was implemented for the eight element linear array at 2.4 GHz.

FIGURE 4.9: Front view of SYNC Unit

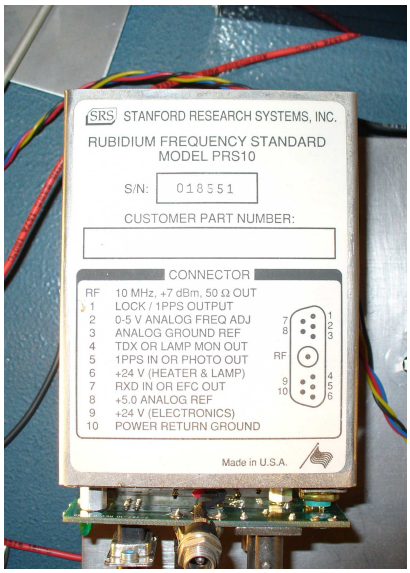

FIGURE 4.10: Rubidium frequency standard

4.4 SYSTEM DEPLOYMENT

4.4.1 Wideband Probing

In order to estimate the channel response at more than a single frequency, the measurement signal must have sufficient bandwidth. Possible choices of wideband excitations include pseudonoise (PN), chirp and multitone signals. The technique typically used in commercial sounders, as well as this current implementation, is the multitone signal, where the number and

FIGURE 4.11: A 2.4 GHz Monopole antenna

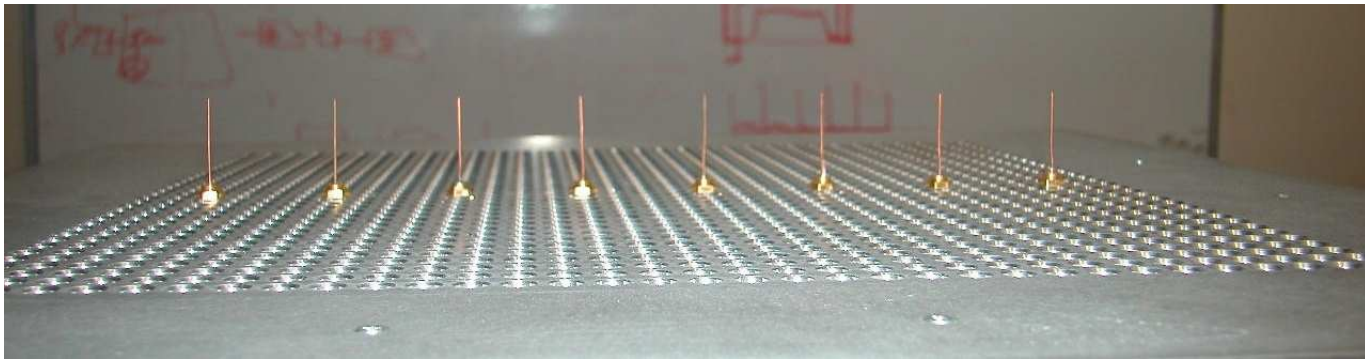

FIGURE 4.12: 2.4 GHz Linear eight element array

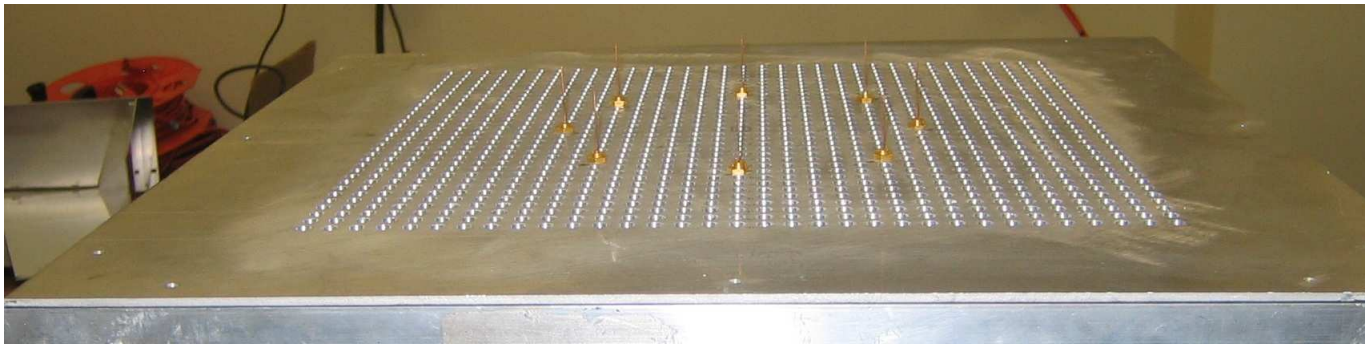

FIGURE 4.13: 2.4 GHz Circular eight element array

FIGURE 4.14: A 5.2 GHz Monopole antenna

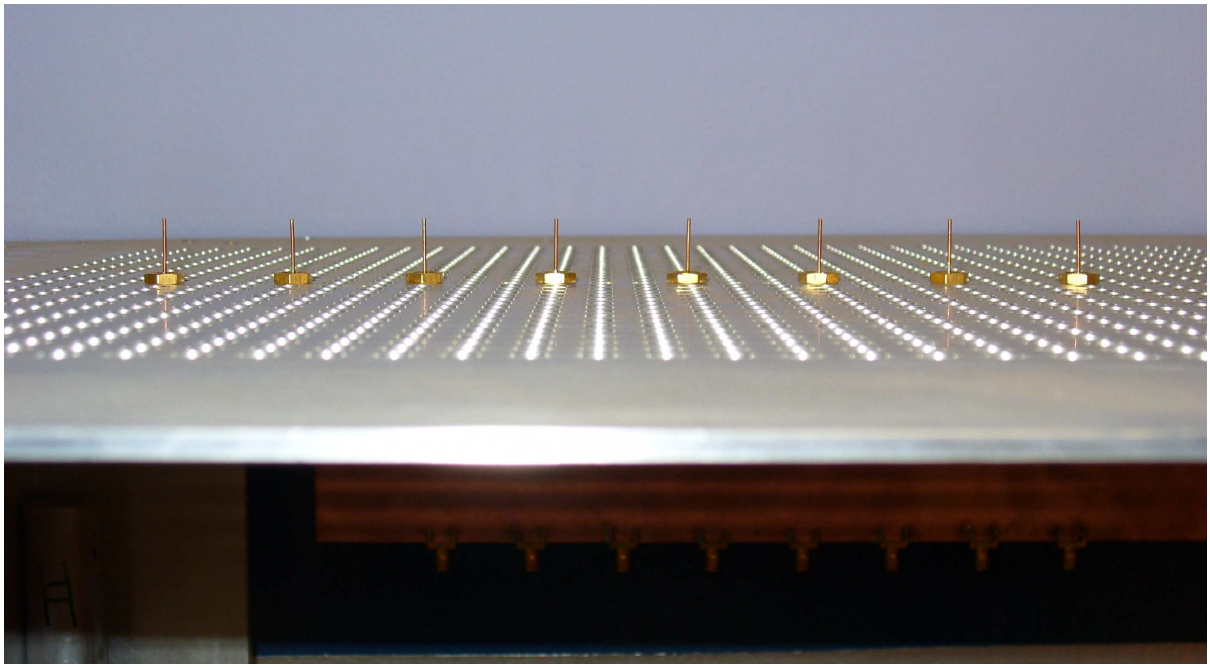

FIGURE 4.15: 5.2 GHz Linear eight element array

FIGURE 4.16: 5.2 GHz Circular eight element array

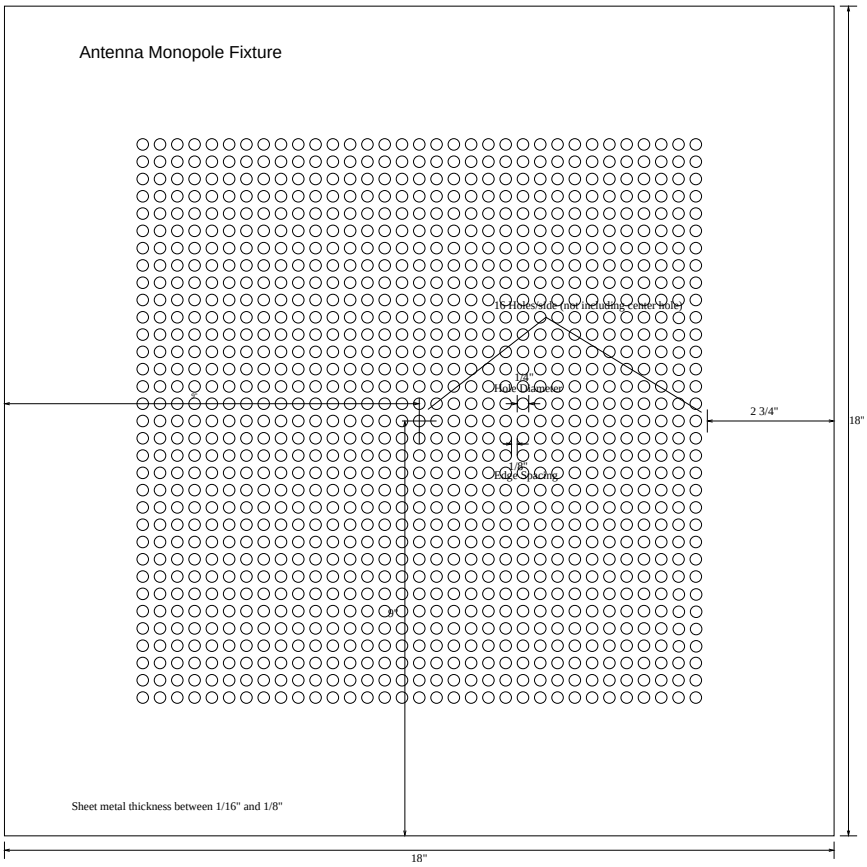

FIGURE 4.17: Grid plate layout for fixing monopole antenna array

spacing of tones can be controlled. In this work, a baseband multitone signal of the form

$$x(t) = \sum_{i=0}^{N_F-1} \cos(2\pi f_i t + \phi_i) \tag{4.1}$$

is used, where f_i and ϕ_i are the frequency and phase of the ith tone, respectively, and for equally spaced tones, $f_i = (i + 0.5)\Delta f$. Note that for each term in (4.1), two tones are created symmetrically about zero frequency, and both tones are present when the signal is up-converted to the microwave carrier. Thus, (4.1) produces $2N_F$ tones with a total probing bandwidth of $(2N_F - 1)\Delta f$. Post processing is simplified if each tone corresponds to a single FFT bin, which is guaranteed when $\Delta f = 2kf_s/N$, where f_s is the sample rate, N is the number of samples in each record and k is an integer.

An obvious advantage of multitone signalling is that the channel response is obtained directly by selecting the appropriate bins of the FFT. One of the drawbacks, however, is that the envelope is not constant, and care must be taken to ensure that the linearity of TX power amplifiers and switches is sufficient to avoid corruption of the measurements. Usually, one

TABLE 4.1: Parameters of the example multitone signal

Parm.	N_F	Δf	T_1	T_2	σ	f_s	N
Value	4	1 MHz	6 μs	7 μs	0.3 μs	400 MS/s	20,000

minimizes the signal's peak-to-average ratio by adjusting the phases of the tones. Here, the phases were optimized by simply selecting a set of random phases uniformly on $[0, 2\pi]$ and retaining the signal with the lowest peak-to-average ratio over many independent realizations.

One consideration with switched measurements is that most PIN-diode switches are not designed for *hot switching*, where high signal level exists during a switching operation. Furthermore, channel estimation is simpler if the acquired signals for the different antenna combinations have no temporal overlap. To avoid hot switching and create separate data records, the multitone signal is multiplied by a Gaussian window of the form

$$w(t) = \begin{cases} e^{-(T_1-t)^2/(2\sigma^2)}, & 0 \leq t < T_1 \\ e^{-(T_2-t)^2/(2\sigma^2)}, & T_2 \leq t \leq T \\ 1, & \text{otherwise}, \end{cases} \tag{4.2}$$

where T_1 and T_2 are the limits of the window, and the standard deviation σ controls the rise and fall time of the window. Typically, the guard time $T_1 + T_2$ is chosen to be much larger than the delay spread of the channel. Guard time also allows the AGC to adapt between switch events.

A simple 8 MHz multitone signal used for outdoor channel probing is depicted in Figure 4.18, with the important parameters listed in Table 4.1. The window spreads the tones slightly, which is unavoidable for a finite-length signal. The active portion of the time-domain signal has a peak-to-average ratio of 1.74, which is close to that of a constant sine wave ($\pi/2 \approx 1.57$).

4.4.2 Calibration Procedure

Since the RF components in the system are not ideal, raw measurements include both the channel and system response. In addition, microwave switches are often constructed with unequal length transmission lines on the various ports, leading to phase errors. These effects can be removed by a careful calibration method.

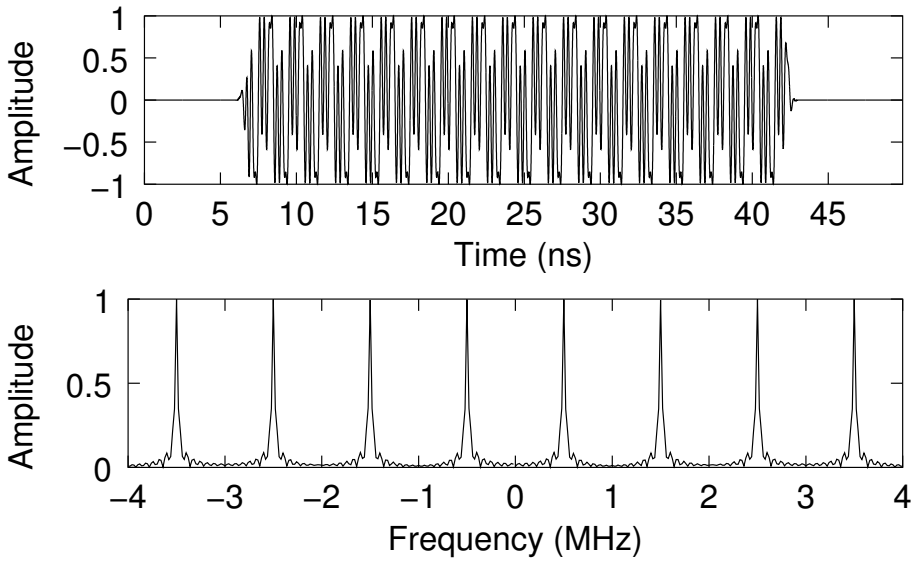

FIGURE 4.18: Example of multitone signal plotted versus time and frequency

Figure 4.19a depicts the measurement setup, where the ideal channel response from the nth TX antenna to the mth RX antenna at baseband frequency f_k is $h_{k,mn}$. One way to accomplish system calibration is to connect TX to RX as depicted in Figure 4.19b, where the switches and antennas have been replaced with a single attenuator with loss L dB. This measurement yields y_k^{cal}, which is the value of the FFT bin corresponding to the baseband tone at frequency f_k. The response of the switches is measured on a network analyzer giving broadband S-parameters $S_{n0}^{\{\text{TX,RX}\}}(f)$, where 0 and n refer to the indices of common and switched ports respectively, and f is the frequency.

Assuming near-linear response from the RX subsystem, a measurement taken with the setup in Figure 4.19a results in

$$y_{k,mn} = L y_k^{\text{cal}} h_{k,mn} S_{0n}^{\text{TX}}(f_k + f_c) S_{0m}^{\text{RX}}(f_k + f_c), \tag{4.3}$$

where k, m, and n are the frequency, RX and TX are indices, and f_c is the carrier frequency. The ideal (or calibrated) channel response h is then obtained from

$$h_{k,mn} = \frac{y_{k,mn}}{L y_k^{\text{cal}} S_{0n}^{\text{TX}}(f_k + f_c) S_{0m}^{\text{RX}}(f_k + f_c)}. \tag{4.4}$$

Another calibration method involves the connection strategy in Figure 4.19c. In this case, the switches remain and the TX and RX are connected via an N_T- and N_R-way power divider and combiner, with measured S-parameters $S_{n0}^{\{\text{TX,RX}\}}(f)$. To avoid RX saturation, a loss of L

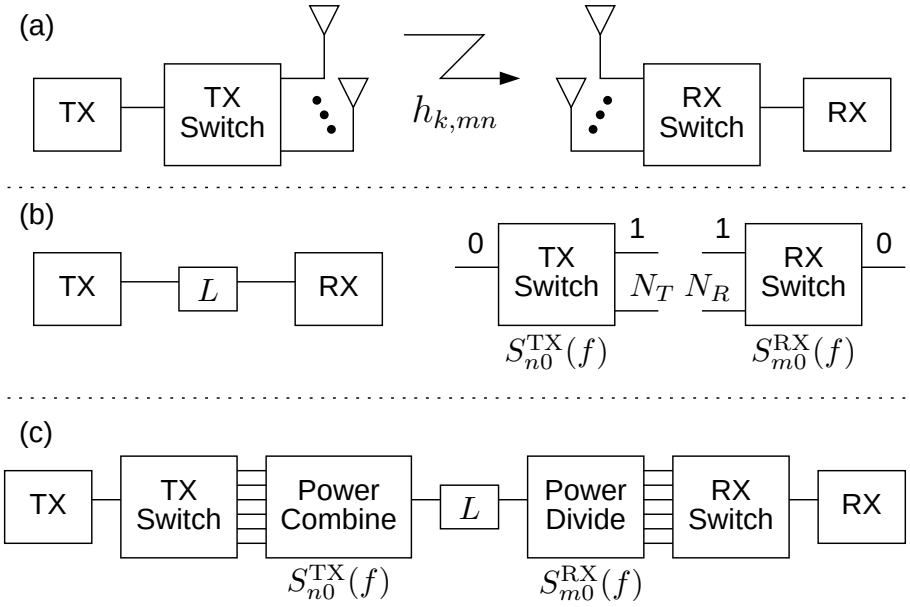

FIGURE 4.19: Procedures for system calibration: (a) original measurement setup, (b) single-channel calibration, and (c) direct matrix calibration

may also be inserted. Measurement of all TX and RX combinations yields $y_{k,mn}^{\mathrm{cal}}$. Similar to the first approach, the ideal channel response is computed as

$$h_{k,mn} = \frac{y_{k,mn} S_{0n}^{\mathrm{TX}}(f_k + f_c) S_{0m}^{\mathrm{RX}}(f_k + f_c)}{L y_k^{\mathrm{cal}}}. \tag{4.5}$$

Note that the position of the S-parameters has changed, since the divider and combiner are present in the calibration, but not the measurement, whereas before the switches were present in the measurement but not the calibration.

The quantity of required calibration information for this procedure can be reduced by noting that the matrix $\mathbf{Y}_k^{cal}$ is rank one, so that $y_{k,mn}^{\mathrm{cal}} = s_k u_{k,m} v_{k,n}^*$, where $\mathbf{u}_k$ and $\mathbf{v}_k$ are the left and right singular vectors associated with the single nonzero singular value s_k for frequency bin k. This rank-one approximation may also improve the calibration accuracy, since information from multiple antennas is averaged.

4.4.3 Measurement Environment

Figure 4.20 depicts the UP system. At the TX side, the antenna array on the grid plate is supported by a pillar which is bolted onto the cart. This provides a good ground plane for the entire system as well. The AWG/microwave source is connected to the RF module which

then feeds the antennas via the SP8T. The rechargeable lead-acid batteries provide 12/24 V so that the rubidium frequency standard, SYNC unit, microwave switches and RF components are continuously powered from a very stable DC source.

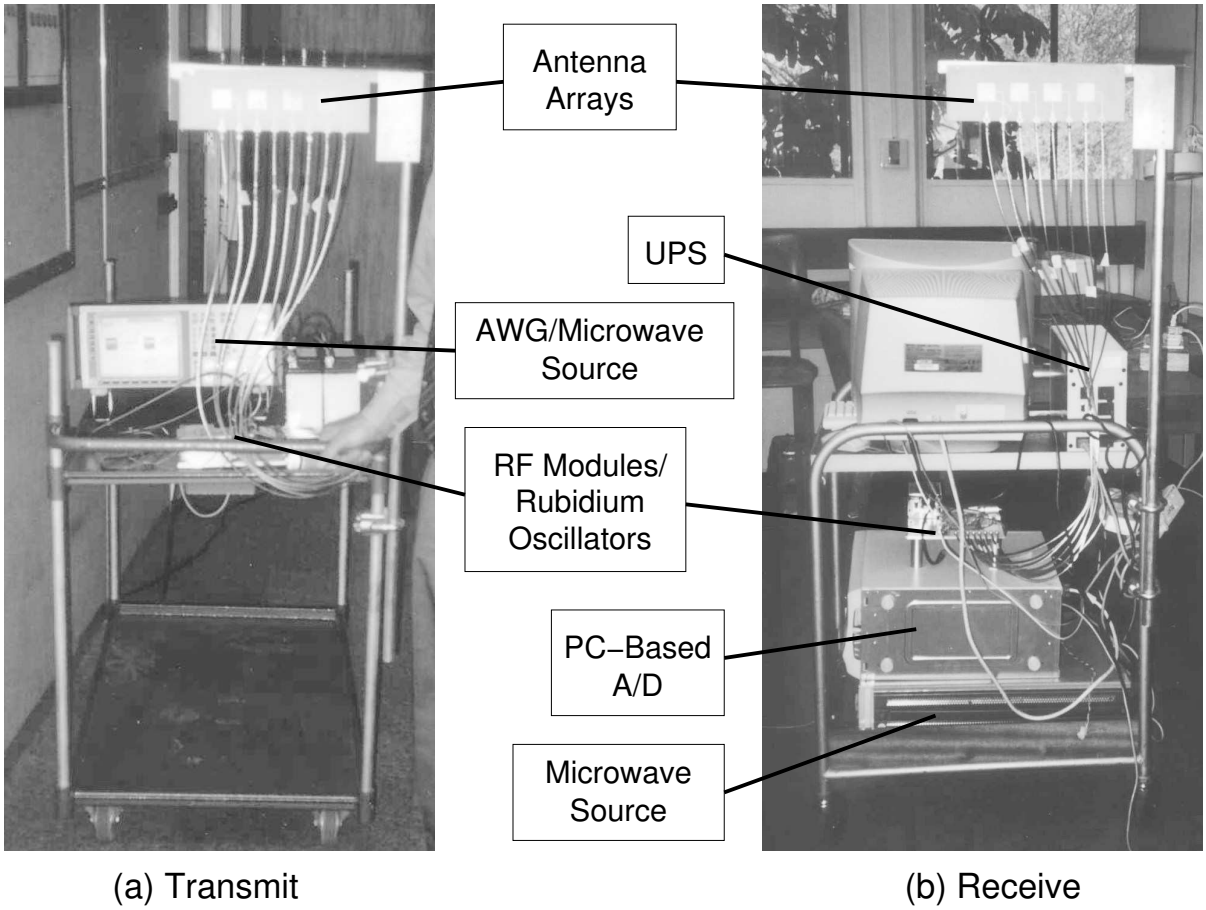

FIGURE 4.20: System constructed and deployed at the University of Pretoria (UP)

At the RX end, an uninterruptible power supply (UPS) provides temporary backup to the PC when the system must be unplugged from the mains for relocation. Here again, the rubidium oscillator and RF module are powered via the 12/24 V rechargeable batteries while the SYNC unit is inside the PC and is powered from the PC power supply.

The measurement campaign performed for this study was done as shown in Figure 4.21 on the first floor in the Carl and Emily Fuchs Institute for Microelectronics (CEFIM) building located on the University of Pretoria (UP) main campus. The TX was fixed at a single position on the central corridor as shown in Fig. 4.21 while the RX was placed at 11 different locations so as to give a good representation of the physical location and its geometry. The TX antennas were

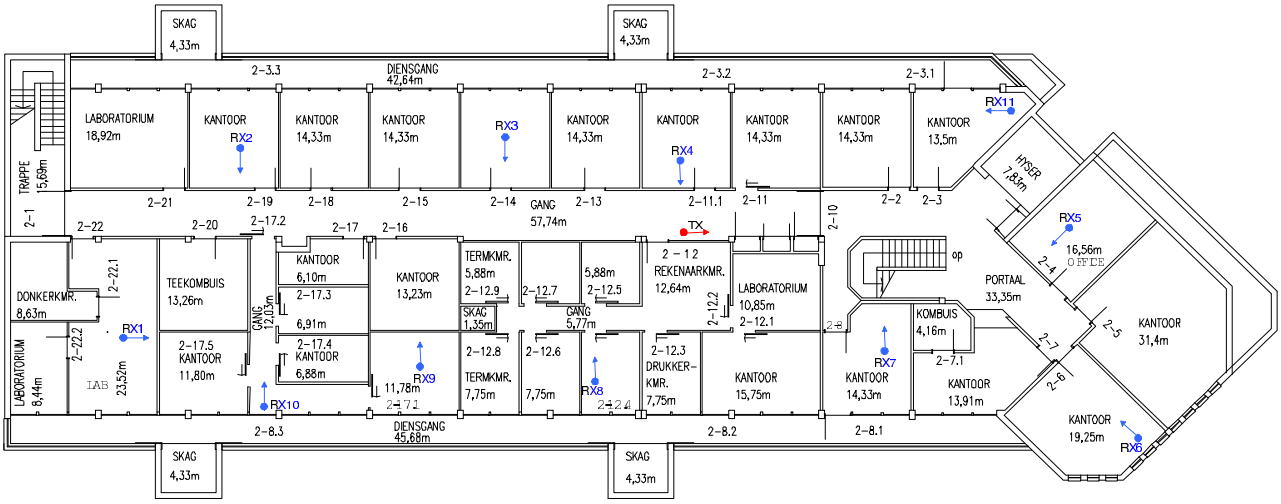

FIGURE 4.21: Measurement scenario in CEFIM at UP

fixed at a height of approximately 1.85 metres and the antenna RX height was approximately 1.5 metres. Co-located MIMO measurements were performed at both 2.4 GHz and 5.2 GHz, meaning that both the TX and RX were at exactly the same geographical position, height and orientation for the 2.4 GHz and 5.2 GHz measurement campaign. This would enable the research, amongst others things, to compare the effect of center frequency on capacity, element correlation, spatial power spectra and other channel modelling characteristics.

4.4.4 Data Collection

In Figure 4.1 the wideband RF signal is routed through the respective port on the SP8T into each of the TX antenna array elements, thus exciting each TX antenna for a total of 20 μs, which consists of 15 μs on time and 5 μs off time. As shown in Figure 4.22, at the receiver another matched SP8T switch, controlled by a SYNC unit synchronized to the one at the TX, routes the incoming RF signal from each of the RX antennas to a common RF receiver. Each RX antenna is connected via the switch for a complete scan of all eight TX antennas, or a total of 160 μs. Thus, a complete scan of the MIMO channel as shown in Figure 4.22 takes 1.28 ms. Since the data acquisition card had limited memory size, approximately 198 ms was allocated for this data to be written onto the hard disk drive of the RX, resulting in a time of 200 ms for one complete 8×8 scan for all TX and RX antennas. In order to improve the accuracy of the results and any variation that may have occurred in the fixed wireless channel, 20 snapshots of the measurement were repeated at each of the 11 locations shown in Figure 4.21, giving us an acquisition time of 4 s. To have a good representation of the channel as well as

sufficient data to capture any impulsive changes at each location, the complete measurement was done twice so that there were at least two snapshots of the complete measurement of the channel at each of the locations. This resulted in the total measurement time of 8 s per location.

Once the raw channel data was captured, the wideband MIMO channel response $\mathbf{H}(\omega)$ for the j^th TX and the i^{th} RX is computed at K=80 discrete frequency bins by dividing the FFT of the captured signal on the j^{th} TX and the i^{th} RX timeslot by the FFT of a calibration signal and selecting bins corresponding to the 80 TX tones. The calibration signal was obtained by connecting the TX and RX through fixed attenuators and performing the measurement as described under the subsection *'Calibration Procedure'*.

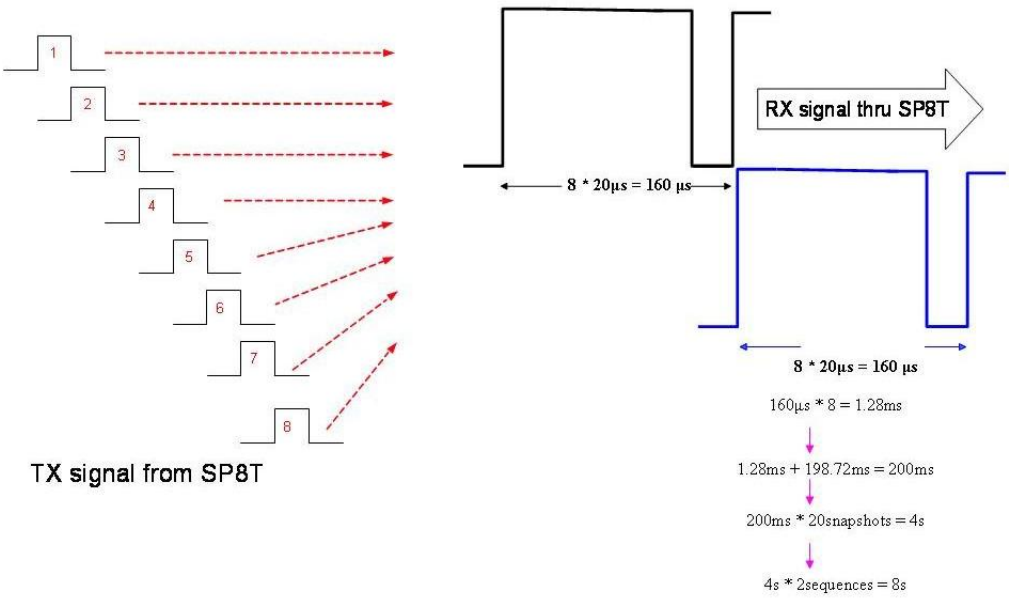

FIGURE 4.22: Switching sequence for measurements at each location

```
H(f,rx,tx,s,ss):
   (f=freq bins,
      rx=RX antennas,
         tx=TX antennas,
            s=sequence no.,
               ss=snapshots)
```

FIGURE 4.23: Channel matrix representation

The channel transfer matrix, **H**, for the channel data is hence formatted in a five dimensional

matrix as shown in Figure 4.23, where the five dimensions are the 80 frequency bins, 8 RX antenna elements, 8 TX antenna elements, 20 sequences of measured data and the 2 snapshots across which all the measurements were acquired respectively. To remove the effect of path loss in all the computations, the channel matrices were normalized according to

$$\tilde{\mathbf{H}}^{(n)} = \left(\frac{1}{N_R N_T N_S} \sum_{m=1}^{N_S} \left\| \mathbf{H}^{(m)} \right\|_F^2 \right)^{-1/2} \mathbf{H}^{(n)} \tag{4.6}$$

where $\tilde{\mathbf{H}}^{(n)}$ and $\mathbf{H}^{(n)}$ are the n^{th} normalized and un-normalized channel matrices respectively. N_s is the number of channel measurements (snapshots and frequency bins) at a single location and $\|\cdot\|_F$ is the Frobenius norm.

4.5 CONCLUSION

Understanding the true channel behavior requires a system capable of direct measurement of the channel. This chapter has introduced the wideband ”switched array” MIMO wireless measurement system as a method of capturing real-world indoor fixed channel behavior, across the 2-6 GHz center frequency band. This chapter presented the hardware and the software techniques for a flexible 8 x 8 MIMO channel measurement system that can probe indoor channels reliably and with accurate repeatability.